Toward Whole-Body Loco-Manipulation: Experimental Results on Multi-Contact Interaction with the Walk-Man Robot

Edoardo Farnioli[1], Marco Gabiccini[1,2,3], Antonio Bicchi[1,2]

***Abstract*— In this paper a quasi-static framework for optimally controlling the contact force distribution is experimentally verified with the full-size compliant humanoid robot Walk-Man. The proposed approach is general enough to cope with multi-contact scenarios, i.e. robot-environment interactions occurring on feet and hands, up to the more general case of *whole-body loco-manipulation*, in which the robot is in contact with the environment also with the internal limbs, with a consequent loss of contact force controllability. Experimental tests were conducted with the Walk-Man robot (i) standing on flat terrain, (ii) standing on uneven terrain and (iii) interacting with the environment with both feet and a hand touching a vertical wall. Moreover, the influence of unmodeled weight on the robot, and the combination with a higher priority Cartesian tasks are shown. Results are presented also in the attached video.**

I. Introduction

One of the main motivations behind the study and the development of high performance humanoid robots is their outstanding potentiality in helping and assisting humans. In legged robots, the presence of the limbs allows the motion of the torso to be largely independent from the roughness of the terrain, improving, in such conditions, their mobility over wheeled robots. An example of challenging scenarios, in which humanoid robots have greater potentiality of success, is in post-disaster environments, where it is necessary to locomote on inclined surfaces, formed e.g. by collapsed walls, and/or to overcome steps or large holes.

Post-disaster scenarios also inspired the past *Darpa Robotics Challenge* (ed. 2015), where the most advanced humanoid robots, such as those in [1], [2], [3] just to mention a few, were called to accomplish tasks such as opening a door, turning a valve, cutting a wall and climbing a ladder.

In order to locomote and balance in unstructured environments, methods based on the Zero-Moment Point (ZMP) [4], also with the appropriate generalization, show their limits, in particular when the robot needs to exploit multiple contacts, e.g. using hands to improve their stability, as in Fig.1.

More general approaches consider the conditions realized on the contact surfaces. Among others, it is worth citing [5], where the authors present a prioritized dynamic control for whole-body tasks in multi-contact scenario. In [6] and [7] the authors use inverse dynamics to minimize the tangential forces, or, more in general, to minimize the difference with a predefined contact force distribution.

[1]Department of Advanced Robotics, Istituto Italiano di Tecnologia, Via Morego 30, 16163 Genova, Italy.

[2]Research Center "E. Piaggio", Università di Pisa, Largo Lucio Lazzarino 1, 56122 Pisa, Italy.

[3]Department of Civil and Industrial Engineering, Università di Pisa, Largo Lucio Lazzarino 1, 56122 Pisa, Italy.

This work is supported by the European Union Seventh Framework Programme [FP7-ICT-2013-10] under grant agreements n.611832 "Walk-Man", and by ERC Advanced Grant no. 291166 "SoftHands" -A Theory of Soft Synergies for a New Generation of Artificial Hands-.

The authors would like to acknowledge Nikolaos Tsagarakis for the valuable support and fruitful discussions.

Fig. 1. The compliant humanoid robot Walk-Man in a multi-contact interaction scenario.

Moving from [8], in [9] the authors propose a contact force optimization with simultaneous posture control. The approach was later extended in [10], with the introduction of a model predictive controller for balancing purposes on a multi-contact scenario.

The approach presented in this paper, tested on the full-size humanoid robot Walk-Man, derives from quasi-static analysis and control tools, initially studied for grasping and manipulation purposes. In [11] and [12], the author discussed the contact force controllability properties of whole-hand grasps, introducing also a metric for evaluating the quality of a contact force distribution. More recently, in [13] and [14], the authors extended the framework in order to properly take into account both the underactuation of the system and the presence of the compliance at different levels. Moreover, the possibility to consider the contact force preload was introduced.

In [15], the authors showed how such tools can be profitably used to find the optimal contact force distribution for compliant humanoid robots in general contact conditions. More precisely, the proposed method, recalled, extended and experimentally verified, respectively in Sec.s II-V, Sec. VI and Sec. VII, differs from other approaches in literature in many ways. The main differences are the following: (i) it directly provides the desired contact force distribution, namely *optimal*, that is the farthest possible from the contact limits, i.e. the minimum and maximum normal force and friction cone constraint, and (ii) it selects the optimal distribution among the set of the contact forces that are actually

controllable. Both characteristics make the proposed method general enough to manage transparently humanoid robots standing on flat terrain, uneven terrain, in a multi-contact situation, i.e. interacting with the environment with feet and hands, up to the most general situation of *whole-body loco-manipulation* [15], [16], [17], in which contacts can occur both on the end-effector and on the internal limbs, with a consequent loss of controllability of some force components.

Experimental results obtained with the compliant humanoid robot Walk-Man are shown both in the paper and in the video footage, for different contact conditions, i.e. standing on flat terrain, standing on uneven terrain and interacting with the environment both with the feet (on flat and on uneven terrain) and with a hand touching a vertical surface. Furthermore, experimental results investigating the influence of (i) an unmodeled weight on the robot, (ii) the combination with a higher priority tasks and (iii) a combination of the previous conditions are shown.

II. Geometric Interpretation of Quasi-Static Approach

A. The Equilibrium Manifold

For space limitations, throughout the paper we will refer to the notation already introduced in [15], Table I. With the symbol $\varphi \in \mathbb{R}^{\sharp\varphi}$ we indicate a vector collecting all the kinematic variables (joint configuration, floating base configuration, etc.) and all the variables involved in the equations of the static equilibrium of the system (joint torques, contact forces, etc.). Let use define the *equilibrium manifold* (EM) of the system as the set of points $\bar{\varphi} : \mathcal{M}(\bar{\varphi}) = 0 \in \mathbb{R}^{\sharp\mathcal{M}}$. Both the dimensions[1] $\sharp\varphi$ and $\sharp\mathcal{M}$ vary depending on the characteristics of the particular system under investigation.

B. The Tangent Space to the Equilibrium Manifold

Given an equilibrium configuration of the system, a first order approximation of the EM can be obtained by means of a Taylor series expansion. Neglecting the contribution of second and higher order terms, the following condition holds for the perturbed configuration

$$\mathcal{M}(\bar{\varphi} + \delta\varphi) \simeq \left.\frac{\partial \mathcal{M}}{\partial \varphi}\right|_{\bar{\varphi}} \delta\varphi := \Phi^{\star}\delta\varphi = 0, \tag{1}$$

which describes the tangent space to the EM.

The matrix $\Phi^{\star} := \left.\frac{\partial \mathcal{M}}{\partial \varphi}\right|_{\bar{\varphi}} \in \mathbb{R}^{r_\Phi \times c_\Phi}$, where $r_\Phi = \sharp\mathcal{M}$ and $c_\Phi = \sharp\varphi$, is the *Fundamental Loco-Manipulation Matrix*[2] (FLMM).

C. Controllable Perturbation of the System

Under the assumption that the FLMM is full row rank, it is possible to split the whole set of kineto-static variables φ in two subsets: the *dependent* variables, and the *independent* variables, denoted as $\varphi_d \in \mathbb{R}^{r_\Phi}$ and $\varphi_i \in \mathbb{R}^{c_\Phi - r_\Phi}$ respectively. The definitions of *dependent* and *independent* variables should be interpreted in the spirit of coordinate partitioning methods used in constrained multibody dynamics algorithms, see [18]. With these definitions, eq. (1) can be rewritten as

$$\begin{bmatrix}\Phi_d^{\star} & \Phi_i^{\star}\end{bmatrix}\begin{bmatrix}\delta\varphi_d \\ \delta\varphi_i\end{bmatrix} = 0, \tag{2}$$

[1]The symbol $\sharp$ is used here to express the cardinality of a set.

[2]The name comes from the analogy with the *Fundamental Grasp Matrix*, initially introduced for the analysis of grasping problem [14].

where $\Phi_d^{\star} \in \mathbb{R}^{r_\Phi \times r_\Phi}$ and $\Phi_i^{\star} \in \mathbb{R}^{r_\Phi \times c_\Phi - r_\Phi}$. Moreover, under the same hypothesis, it is possible to choose φ_i and φ_d such that the matrix $\Phi_d^{\star}$ is invertible. As a consequence, (2) can be left-multiplied by $\Phi_d^{\star -1}$ obtaining

$$\Phi\delta\varphi := \begin{bmatrix}I & \Phi_i\end{bmatrix}\begin{bmatrix}\delta\varphi_d \\ \delta\varphi_i\end{bmatrix} = 0, \tag{3}$$

where $\Phi_i := \Phi_d^{\star -1}\Phi_i^{\star}$. The new coefficient matrix $\Phi \in \mathbb{R}^{r_\Phi \times c_\Phi}$ is the *canonical form of the Fundamental Loco-Manipulation Matrx* (cFLMM). From (3) it follows that

$$\delta\varphi_d = -\Phi_i\delta\varphi_i. \tag{4}$$

III. System Description

Let us show how the elements composing (2) and (3) can be computed for the case of a compliant humanoid robot in a *whole-body loco-manipulation* task, as sketched in Fig. 2.

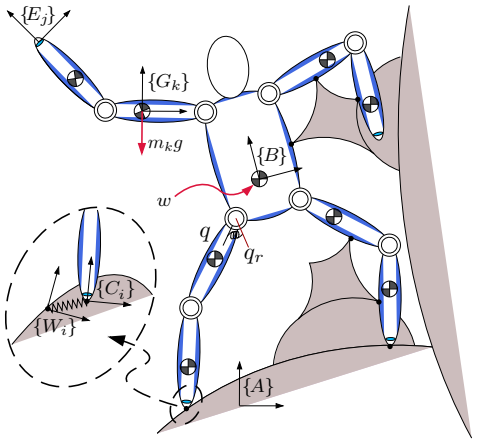

Fig. 2. Reference scenario for compliant humanoid robot in *whole-body loco-manipulation* task.

A. Humanoid Robot

Between the absolute frame $\{A\}$ and the floating base of the robot $\{B\}$, we introduce a virtual kinematic chain (VKC), able to fully parametrize their mutual configuration. With the symbols $u \in \mathbb{R}^6$ and $q \in \mathbb{R}^{\sharp q}$ we indicate the joint variables of the VKC and of the robot, respectively. A vector collecting both the variables will be indicated as $q^* = \begin{bmatrix}u^T & q^T\end{bmatrix}^T \in \mathbb{R}^{6+\sharp q}$.

On the i^{th} of c contacts, we consider a linear spring whose extremities are connected to the world $\{W_i\}$ and to the robot $\{C_i\}$ contact frames, respectively. We consider here that only the three components of linear forces, and no moments, can be transmitted through the contacts. However, the generalization poses no difficulties.

Finally, in the center of mass of the k^{th} of l links, we place the origin of a reference frame $\{G_k\}$, with orientation always parallel to $\{A\}$.

With the symbol $\xi \in \mathbb{R}^{\sharp\xi}$, with $\sharp\xi = 3c + 3l$, we indicate a vector collecting all the linear velocities of the frames $\{C_i\}$ and $\{G_k\}$ expressed in local coordinates. With these definitions we can write

$$\xi = J^*\dot{q}^* := \begin{bmatrix}S_h^T & J_h\end{bmatrix}\begin{bmatrix}\dot{u} \\ \dot{q}\end{bmatrix}, \tag{5}$$

where $J^* \in \mathbb{R}^{\sharp\xi \times \sharp q^*}$ is the complete Jacobian of the robot, including the VKC, $S_h \in \mathbb{R}^{6 \times \sharp\xi}$ is the *stance matrix*, and $J_h \in \mathbb{R}^{\sharp\xi \times \sharp q}$ is the *humanoid Jacobian matrix*. It is worth

noting that the above definitions recall those introduced in [19]. The velocities of the contact frames and of the CoM frames can be pointed out writing

$$\begin{bmatrix}\xi_c\\ \xi_g\end{bmatrix} = \begin{bmatrix}S_c^T & J_c\\ S_g^T & J_g\end{bmatrix}\begin{bmatrix}\dot{u}\\ \dot{q}\end{bmatrix}, \tag{6}$$

with evident definition of the symbols.

By kineto-static duality arguments, from (5) we can obtain the equilibrium condition for the whole robot, including the VKC, as

$$\tau^* = J^{*T}\lambda, \tag{7}$$

where $\lambda \in \mathbb{R}^{3c+3l}$ is a vector collecting all the contact forces, $f_c \in \mathbb{R}^{3c}$, and the gravitational forces acting on the CoM of each robot link, collected in the vector $m_g \in \mathbb{R}^{3l}$. Formally, this can be written as $\lambda = \begin{bmatrix}f_c^T & -m_g^T\end{bmatrix}^T$, where signs are introduced so that forces exerted by the robot on the environment are positive.

In (7), the symbol $\tau^* \in \mathbb{R}^{(\sharp q+6)}$ indicates a vector collecting the virtual torques applied to the joints of the VKC, indicated as $w \in \mathbb{R}^6$, and the robot joint torques, $\tau \in \mathbb{R}^{\sharp q}$. It is worth noting that the vector w can be considered as a parametrization of an external wrench acting on the floating base of the robot.

By differentiation, considering that there is no variation of the gravitational forces in local frames, from (7) we can obtain the quasi-static form of the equilibrium of the robot. With reference to the matrices introduced in (6), we obtain

$$\delta w = S_c\delta f_c + U_s\delta u + Q_s\delta q, \tag{8}$$

$$\delta\tau = J_c^T\delta f_c + U_j\delta u + Q_j\delta q, \tag{9}$$

where $U_s = \frac{\partial S_h\lambda}{\partial u}\big|_{\bar{\varphi}} \in \mathbb{R}^{6\times 6}$, $Q_s = \frac{\partial S_h\lambda}{\partial q}\Big|_{\bar{\varphi}} \in \mathbb{R}^{6\times\sharp q}$, $U_j = \frac{\partial J_h^T\lambda}{\partial u}\Big|_{\bar{\varphi}} \in \mathbb{R}^{\sharp q\times 6}$ and $Q_j = \frac{\partial J_h^T\lambda}{\partial q}\Big|_{\bar{\varphi}} \in \mathbb{R}^{\sharp q\times\sharp q}$. As explained, the set of eq.s (8) and (9) provides a description of the quasi-static equilibrium of the robot.

B. Compliant Joints

In order to safely absorb impacts, modern humanoid robots are often designed with a certain amount of physical compliance. This feature can be modeled introducing the joint stiffness matrix $K_q \in \mathbb{R}^{\sharp q\times\sharp q}$, collecting all the joint stiffness values, and the motor position vector, $q_r \in \mathbb{R}^{\sharp q}$. With these definitions, the quasi-static form for the equilibrium of the elastic joints can be written as

$$\delta\tau = K_q(\delta q_r - \delta q). \tag{10}$$

C. Constitutive Equation of the Contact

Indicating with p_{wc}^c a vector collecting all the position of the frames $\{C_i\}$ with respect to $\{W_i\}$, with coordinates in $\{C_i\}$, and considering the virtual spring at the contacts, the force vector can be computed as $f_c = K_c p_{wc}^c$, where $K_c \in \mathbb{R}^{3c\times 3c}$ is the contact stiffness matrix. By differentiation, with reference to the expression for the contact frame displacements in (6), the contact force variation can be written as

$$\delta f_c = K_c(S_c^T\delta u + J_c\delta q). \tag{11}$$

IV. Quasi-Static Control of the System

The set of eqs. (8), (9), (10) and (11) can be casted in the form (1), whose blocks take the form

$$\Phi^\star = \begin{bmatrix} I_f & 0 & -K_cS_c^T & -K_cJ_c & 0 & 0\\ -J_c^T & I_\tau & -U_j & -Q_j & 0 & 0\\ -S_c & 0 & -U_s & -Q_s & I_w & 0\\ 0 & I_\tau & 0 & K_q & 0 & -K_q\end{bmatrix}, \tag{12}$$

$$\delta\varphi = \begin{bmatrix}\delta f_c^T & \delta\tau^T & \delta u^T & \delta q^T & \delta w^T & \delta q_r^T\end{bmatrix}^T. \tag{13}$$

Under the assumption that the first square block of (12) is full rank[3], it is possible to choose the external wrench variation and the joint reference displacement as the *independent* variables. Left multiplying the system by $\Phi_d^{\star-1}$, we finally obtain (3), from which we can extract the relationship between the k^{th} *dependent* variable and the *independent* ones in the form

$$\delta\varphi_{d_k} = -W_{d_k}\delta w - R_{d_k}\delta q_r. \tag{14}$$

If no external disturbance is acting on the robot ($\delta w = 0$), from (14), it follows that the contact force variation can be expressed as

$$\delta f_c = -R_f\delta q_r := Ey, \tag{15}$$

where $E \in \mathbb{R}^{\sharp f\times\rho_{R_f}}$, with $\rho_{R_f} = \text{rank}(R_f)$, represents a basis for the controllable contact forces, and $y \in \mathbb{R}^{\rho_{R_f}}$ is a suitable coefficient vector.

V. Optimal Contact Force Distribution

In order to choose a proper contact force distribution between the set of the controllable ones, described by the matrix E in (15), let us consider the contact force limits. More in details, for the i^{th} contact point, the constraints imposing the *maximum* and *minimum normal force*, and the compatibility with the *friction cone* can be compactly described by the following inequalities

$$\sigma_{i,j} = \alpha_{i,j}\|f_{c_i}\| + \beta_{i,j}f_{c_i}^T n_i + \gamma_{i,j} \le 0, \tag{16}$$

where $j = \{\max, \min, \text{frict}\}$. In Table I, the values of the coefficients are summarized for the different cases.

Choosing an arbitrarily small positive quantity ε, such that the approximation $\sigma_{i,j} \le -\varepsilon$ is acceptable for (16), for the i^{th} contact point and for the j^{th} contact constraint, we introduce the function

$$V_{i,j} = \begin{cases} (2\sigma_{i,j}^2)^{-1} & \text{if } \sigma_{i,j} < -\varepsilon,\\ a\,\sigma_{i,j}^2 + b\,\sigma_{i,j} + c & \text{otherwise.}\end{cases} \tag{17}$$

By imposing continuity conditions, we can find $a = \frac{3}{2\varepsilon^4}$, $b = \frac{4}{\varepsilon^3}$, $c = \frac{3}{\varepsilon^2}$.

	$\alpha_{i,j}$	$\beta_{i,j}$	$\gamma_{i,j}$
frict	$\alpha_i > 0$	-1	0
min	0	-1	$f_{\min_i}$
max	0	1	$-f_{\max_i}$

TABLE I

Coefficient values for contact constraints in (16); $\alpha_{i,j}$ is related with the friction coefficient $\mu_{i,j}$ by $\alpha_{i,j} = 1/\sqrt{1+\mu_{i,j}^2}$.

[3]This can be demonstrated in simple cases and it was also numerically verified in many other cases, without finding exception. This bring to consider this assumption reasonable at least for the usual cases of interest. Moreover, the assumption can be easily verified with an online check of the rank during the application.

With the previous definitions and observing that, by means of (15), the elements $\sigma_{i,j}$ are functions of the coefficient vector y, the scalar function

$$V = \sum\nolimits_{i,j} V_{i,j} \tag{18}$$

can be associated to a contact force variation and, considering the initial forces, to a *new* contact force distribution.

We can also note that, by construction, lower values of V correspond to a contact force distribution that is globally more distant to the contact limits.

Avoiding a detailed discussion, for which the interested reader is referred to [15], we just recall here the result that the function $V(y)$ in (18) is *strictly convex*. In consequence of that and of the previous observation, we can conclude that the minimum of V corresponds to the *optimal* contact force distribution, along the metrics defined by (16), in terms of global distance to the contact limits. Therefore, the optimal contact force variation can be computed as

$$\delta f_c^{\text{opt}} = E y^{\text{opt}} : y^{\text{opt}} = \text{argmin}\left(V\left(y\right)\right). \tag{19}$$

From (15) , the corresponding joint reference displacement to be applied results in

$$\delta q_r^{\text{opt}} = -R_f^{\dagger} \delta f_c^{\text{opt}}. \tag{20}$$

VI. Prioritized Realization of Kineto-Static Tasks

For later use, with the symbol $P_{\mathcal{N}(A)}$ we indicate a projector in the nullspace of A, which can be computed as $P_{\mathcal{N}(A)} = \left(I - A^{\dagger} A\right)$.

Let us consider the case in which a second task to accomplish is specified in Cartesian space, i.e. in terms of posture of an end-effector (e.e.) frame $\{E_j\}$, Fig. 2. From the differential kinematics, for the e.e. displacement we can easily obtain

$$\delta C_e = \begin{bmatrix} S_e^T & J_e \end{bmatrix} \begin{bmatrix} \delta u \\ \delta q \end{bmatrix}. \tag{21}$$

However, eq. (21) is not expressed in terms of independent variables of the system, thus it can not be directly combined with (15). To face this situation, we can consider (14), evaluated for the case of the floating frame and the robot joint displacements. If no external disturbance is acting on the robot, respectively we obtain $\delta u = -R_u \delta q_r$ and $\delta q = -R_q \delta q_r$. Substituting these in (21) we obtain

$$\delta C_e = -\left[S_e^T R_u + J_e R_q\right] \delta q_r := -R_e \delta q_r. \tag{22}$$

With this formulation, eq.s (22) and (15) can be properly combined for achieving the relative tasks with the desired order of priority. For example, giving maximum priority to the force realization task we can write

$$\delta q_r^{\text{des}} = -R_f^{\dagger} \delta f_c^{\text{des}} - P_{\mathcal{N}(R_f)} R_e^{\dagger} \delta C_e^{\text{des.}} \tag{23}$$

Conversely, if the kinematic task on the e.e. has higher priority, the solution can be computed in the form

$$\delta q_r^{\text{des}} = -R_e^{\dagger} \delta C_e^{\text{des}} - P_{\mathcal{N}(R_e)} R_f^{\dagger} \delta f_c^{\text{des}}. \tag{24}$$

VII. Experimental Results with Walk-Man Robot

A. The Walk-Man Robot

The method presented above was tested on the Walk-Man robot, a full-size compliant humanoid robot developed jointly by the Italian Institute of Technology and the University of Pisa. The robot participated to the 2015 edition of the Darpa Robotic Challenge (DRC), completing the car driving task and the door opening task, before coming to a halt caused by battery issues. An image of the robot is shown in Fig. 1. The humanoid is approximately 1.9m tall, from the foot sole to the head top. In the configuration used during the tests of this paper, the total weight of the Walk-Man robot was approximately 120kg. The robot has a total of 33 DoF, 6 for each leg, 7 for each arm, 3 for the torso, 2 for the neck, 2 for the closure of the Pisa/IIT SoftHands [20]. The control PC is based on a $i7$ Quad-Core processor running at variable frequency in the range 1.7–2.8GHz. The control loop period used was 50ms. The stiffness at the joints have the values $k_q = 10000$Nm/rad for the high-power joints, located in the legs and in the torso, $k_q = 1000 - 6000$Nm/rad for the medium-power joints, located in the first 4 joints of the arms, $k_q = 500$Nm/rad, for the low-power joints, the last 3 joints of the arms. More details on the hardware design of the robot can be found in [21].

Considering the rubber covering the contact surfaces on the feet and on the hands the contact stiffness was set to $k_c = 10^6$N/m. For each link of the robot (foot or hand) in contact with the environment 4 contact forces were considered. The actual components of the contact forces were computed at every loop by means of the pseudoinverse of the proper grasp matrix, mapping the contact forces on the corresponding frame of 6−axis force/torque sensor, located in the foot sole and in the wrist. To the obtained measures, a low-pass filter was applied by means of a windowing function with dimension of 15 samples. The application of (20) was made by means of the damped pseudoinverse, with damping factor $d^2 = 10^7$.

Indicating with μ_l the friction coefficient on the left foot and with μ_r the friction coefficient on the right foot, in order to compute the function V in (18), three different friction conditions were considered: (i) $\mu_l = \mu_r = 1$, (ii) $\mu_l = 1,\ \mu_r = 0.2$ and (iii) $\mu_l = 0.2,\ \mu_r = 1$. The corresponding optimal contact force distribution was computed offline, using a simplified model, similar to the one used in [15] for numerical tests, adapted in the kineto-static parameters for the case of the Walk-Man Robot. The resulting optimal contact force distribution can be approximated as equal distribution of the weight on the two feet, for the case (i), and 85% of the weight on the foot with lower friction, 15% of the weight on the foot with higher friction, for the cases (ii) and (iii).

B. Experimental Results

Flat Terrain: In the first experiment the Walk-Man robot initially stands on flat terrain, as in Fig. 3(a).

Fig.s 3(b), 3(c), 3(d) show the final configuration achieved by the robot following the optimal contact force distribution, computed for the friction conditions (i), (ii) and (iii), respectively. The corresponding error evolutions are shown in Fig. 4. On the y axis the error $e_f = \|\delta f_c\|$, i.e. the norm of the difference between the actual and the desired contact force distribution, is shown. Note that, when only feet are in contact, $\delta f_c \in \mathbb{R}^{24}$. On the x axis the number of the samples is represented. Samples are taken every 50ms.

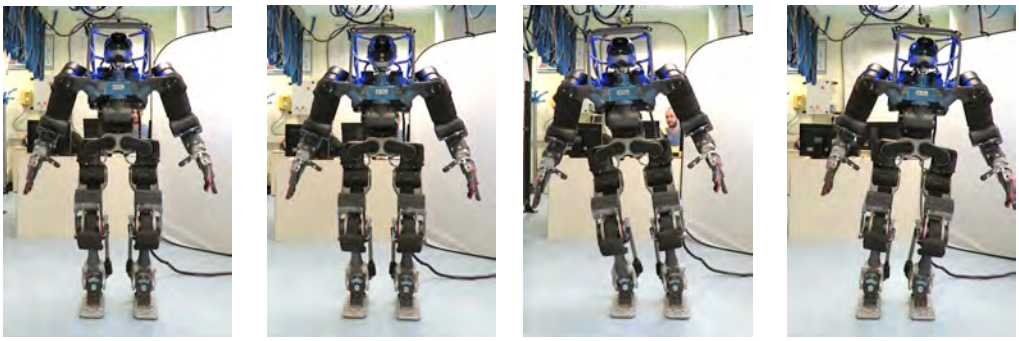

(a) Initial Configuration (b) $\mu_l = 1$, $\mu_r = 1$ (c) $\mu_l = 1$, $\mu_r = 0.2$ (d) $\mu_l = 0.2$, $\mu_r = 1$

Fig. 3. Experimental tests on flat terrain. Friction values used are specified in subcaptions. In Panel(a) the initial configuration of the robot is shown. Panels (b)-(d) show the final configuration of the robot achieved in the test for meeting the optimal contact forces.

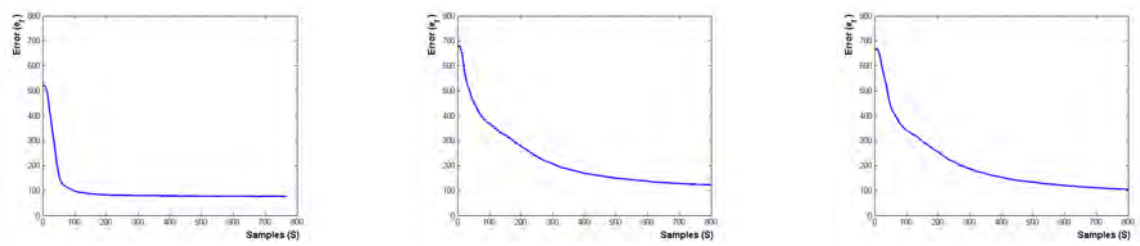

(a) Error evolution relative to Fig. 3(b) (b) Error evolution relative to Fig. 3(c) (c) Error evolution relative to Fig. 3(d)

Fig. 4. Error evolution graph relative to the experiments in Fig. 3. Error $e_f = \|\delta f_c^{\text{des}}\|$; samples taken every 50ms.

Uneven Terrain: The same friction conditions were considered also on uneven terrain, represented in Fig. 5. The inclination of the surfaces with respect to the horizontal plane are of 15° for both the feet. In the initial configuration, Fig. 6(a), the robot feet are not at the same level, and the lateral edges of the right and of the left foot are not parallel.

Fig. 5. Uneven terrain used for tests. The surfaces are inclined of 15° with respect to a horizontal plane.

The experimental results, in terms of final configuration of the robot and of error evolution, are represented in Fig.s 6(b)-(d) and in Fig. 7, respectively. By direct comparison of Fig. 4 and 7, we can note that the main difference between the performance obtained on flat and on uneven terrain is in the response time, slower in the case of uneven terrain. However, it results also that there is a limited difference between the steady-state errors in the two cases. Numerically, for the case (i) the minimum error is $e_f^{\min} = 75$N on flat terrain and $e_f^{\min} = 73$N on uneven terrain ($\simeq$ 3N/force component); for the case (ii) $e_f^{\min} = 117$N on flat terrain and $e_f^{\min} = 212$N on uneven terrain; for the case (iii) $e_f^{\min} = 101$N on flat terrain and $e_f^{\min} = 166$N on uneven terrain. We can also note that, where the difference is much relevant, as in case (ii), greater is also the difference in the derivative of the error, suggesting that, on uneven terrain, the minimum error is not achieved yet at the end of the test. In all the cases, the steady-state error seams to be compatible with errors in the model and in the measurements.

Influence of Other Contributions: In order to investigate the influence of other actions on the error evolution, the experiments on flat and uneven terrain were repeated considering the friction condition (iii). In the first test, Panel (a) of Fig.s 8 and 10, an unmodeled mass of 2kg was introduced, in correspondence of the right wrist. From direct comparison of the error evolution in Fig. 9(a) and Fig. 11(a) with their counterpart without additional weight in Fig. 4(c) and Fig. 7(c), we can observe that the unmodeled weight contribute in making the convergence slower toward the minimum error. After 500 samples (30 sec.s) the error is $e_f^{\min} = 137$N, against the $e_f^{\min} = 131$N, without the weight. Similarly, on uneven terrain, after 500 samples in this case the error is $e_f^{\min} = 235$N, against $e_f^{\min} = 201$N in the corresponding experiments without the unmodeled weight.

In the cases represented in Fig.s 8(b) and 10(b) the desired joint reference displacement resulting from (20), were projected in the nullspace, by means of (24), of the Jacobian obtained as the stack of the right hand and of the right foot Jacobian. In consequence of this, both the right hand and the right foot do not move in the Cartesian space during the test. If for the right hand this consequence can be directly observed, it is interesting to note that imposing no motion to the right foot forbids small movements, able to deform the contact rubber, difficult to see in usual condition, whose effect actually contributes to the minimization of the error. This can be observed comparing Fig. 9(b) and Fig. 11(b) with Fig. 4(c) and Fig. 7(c), respectively.

Finally, in the tests represented in 8(c) and 10(c), both the unmodeled weight and the nullspace projection were used. From the graphs of the errors, presented in Fig. 9(c) and in 10(c), it appears that both contribute to the decay of the performances.

Multiple contacts: In Fig.s 12 and 13, two photo sequences are presented, showing the Walk-Man robot preserv-

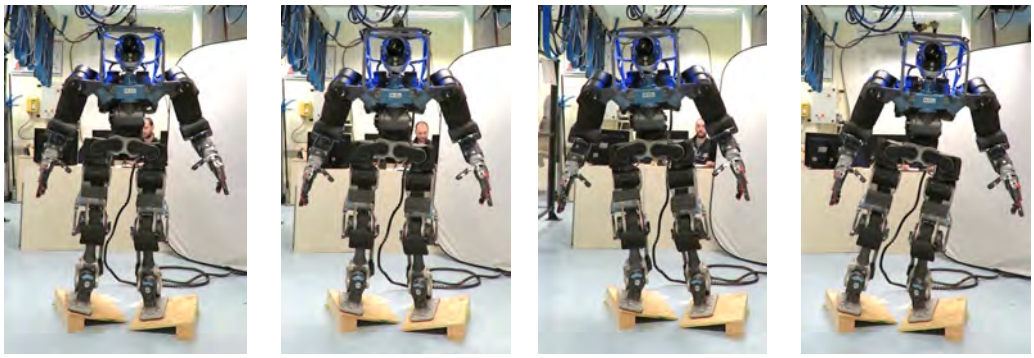

(a) Initial Configuration (b) $\mu_l = 1$, $\mu_r = 1$ (c) $\mu_l = 1$, $\mu_r = 0.2$ (d) $\mu_l = 0.2$, $\mu_r = 1$

Fig. 6. Experimental tests on uneven terrain. Friction values are specified in subcaptions. Panels (b)-(d) show the final configuration of the robot for meeting the optimal contact forces. Panels (b)-(d) show the final configuration of the robot achieved in the test for meeting the optimal contact forces.

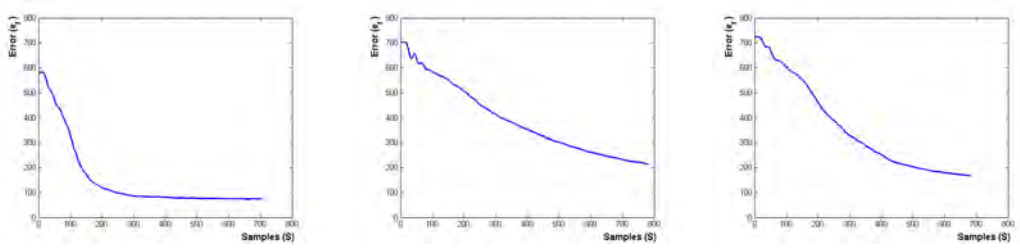

(a) Error evolution relative to Fig. 6(b) (b) Error evolution relative to in Fig. 6(c) (c) Error evolution relative to Fig. 6(d)

Fig. 7. Error evolution relative to Fig. 6. Error $e_f = \|\delta f_c^{\text{des}}\|$; samples taken every 50ms.

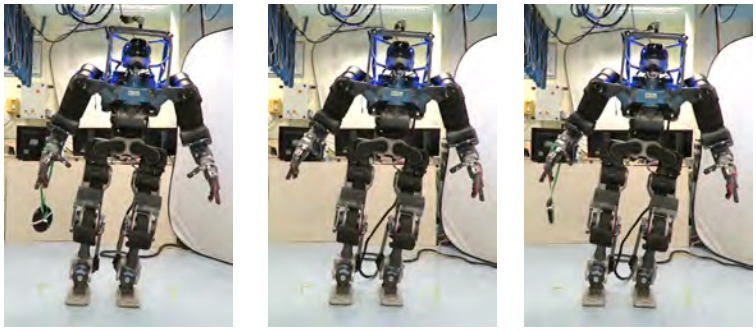

(a) Unmodeled Weight (b) Nullspace Projection (c) Unmodeled Weight + Nullspace Projection

Fig. 8. In these tests the friction coefficient are set to $\mu_l = 0.2$, $\mu_r = 1$. In Fig. 8(a) the test was performed adding a 2kg unmodeled weight on the right wrist. In Fig. 8(b) the joint reference variation resulting from (20) was projected in the nullspace of the Jacobian of the right hand and of the right foot by means of (24). In the experiment in Fig. 8(c) both the unmodeled weight and the nullspace projection were introduced.

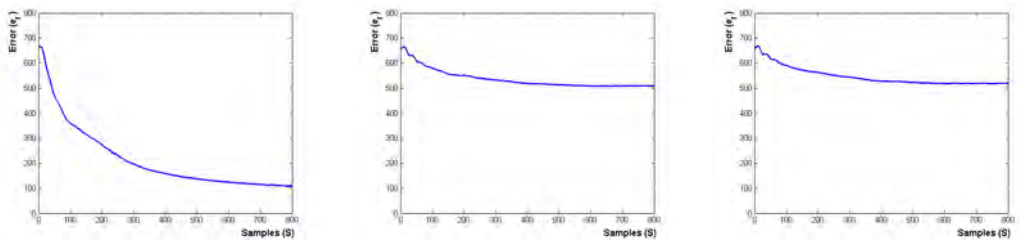

(a) Error evolution relative to Fig. 8(a) (b) Error relative to Fig. 8(b) (c) Error evolution relative to Fig. 8(c)

Fig. 9. Error evolution relative to Fig. 8. Error $e_f = \|\delta f_c^{\text{des}}\|$; samples taken every 50ms.

ing the stance condition while changing the contact points: from standing on the feet, to keeping the equilibrium with one foot on the ground and one hand touching a vertical surface. In the first case, Fig. 12, the floor is flat, in the second one, Fig. 13, the feet are located on an uneven terrain composed by two inclined surfaces, represented in Fig. 5.

In both the cases, initially (Panels (a) and (b)) the hand of the robot is not in contact with the environment. When the robot comes in touch with the wall (Panels (c)), the operator starts the contact force optimization module. In these cases, the desired contact forces were imposed to be equal to the 85% of the weight on the left foot, in direction normal to the ground, zero force for all the components of the right foot, and the 15% of the weight as reaction force on the right hand,

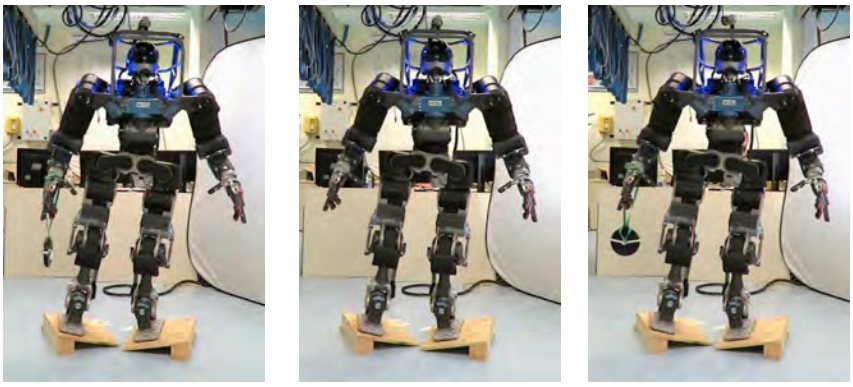

(a) Unmodeled Weight (b) Nullspace Projection (c) Unmodeled Weight + Nullspace Projection

Fig. 10. In these tests the friction coefficient are set to $\mu_l = 0.2$, $\mu_r = 1$. In Fig. 8(a) the test was performed adding a 2kg unmodeled weight on the right wrist. In Fig. 8(b) the joint reference variation resulting from (20) was projected in the nullspace of the Jacobian of the right hand and of the right foot by means of (24). In the experiment in Fig. 8(c) both the unmodeled weight and the nullspace projection were introduced.

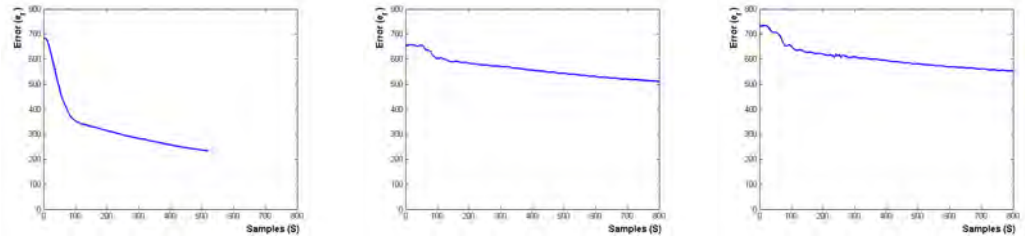

(a) Error evolution relative to Fig. 10(a) (b) Error evolution relative to Fig. 10(b) (c) Error evolution relative to Fig. 10(c)

Fig. 11. Error evolution graph relative to the experiments in Fig. 10. Error $e_f = \|\delta f_c^{\text{des}}\|$; samples taken every 50ms.

in direction normal to the wall. All the desired tangential forces are set to zero. Note that, in this case, the desired contact force distribution can not be achieved, since they do not correspond to any equilibrium condition of the robot. For each contact surface, similarly to the previous cases, 4 contact forces were considered, for a total of 36 components of force.

When the normal reaction on the right foot decreases sufficiently (approximately less than the 10% of the weight) the operator switches control mode (Panels (c) and (d) of Fig.s 12 and 13), applying a whole-body inverse kinematics algorithm, based on the pseudoinverse of proper Jacobian matrices, asking to satisfy the tasks of lifting up the right foot, and of keeping the configuration of the left foot, of the hands and of the CoM of the robot.

The error evolutions of the contact forces, registered when the contact force optimization module is running, are shown in Fig.s 14(a) and 14(b), respectively for the tests in Fig.s 12 and 13.

The relatively high values of the error at the final stage (when the contact force optimization module is arrested) are caused by the fact that: (i) not all the force components can be actually achieved, (ii) the switch is made just considering the conditions on the right foot, not on the other contacts. However, it is worth noting that, despite that the desired force vector cannot be achieved, the application of the proposed method still shows a robust behavior, imposing in any case a negative time derivative of the error.

VIII. Conclusions

In this paper we presented a quasi-static framework for the analysis and control of compliant humanoid robot under general multi-contact conditions, able to cope also with *whole-body loco-manipulation* tasks. A geometrical interpretation of the method was presented before discussing the system of equations more in detail. Then, the *dependent* and *independent* variables of the system were defined, together with a systematic method for exploiting them, able to provide a basis for the controllable movements of the robot, as well as for the controllable contact forces. A convex function was used to find the *optimal* controllable contact force distribution, in terms of distance from the contact limits. Experimental tests were conducted with the WalkMan robot in different contact conditions and considering different friction values. The proposed method was tested with the robot (i) standing on flat terrain, (ii) standing on uneven terrain and (iii) interacting with the environment both with the feet and with one hand, in contact with a vertical wall. Moreover, the influence of (additional) errors in the model was tested introducing an unmodeled weight on the robot. The prioritized combination with a Cartesian task was finally verified both with and without the additional unmodeled weight, as also reported in the attached video.

References

[1] H. Wang, Y. F. Zheng, Y. Jun, and P. Oh, "Drc-hubo walking on rough terrains," in *Technologies for Practical Robot Applications (TePRA), 2014 IEEE International Conference on*, pp. 1–6, April 2014.

[2] P. Hebert, M. Bajracharya, J. Ma, N. Hudson, A. Aydemir, J. I. Reid, C. Bergh, J. Borders, M. Frost, M. Hagman, J. Leichty, P. Backes, B. Kennedy, P. Karplus, B. W. Satzinger, K. Byl, K. Shankar, and J. W. Burdick, "Mobile manipulation and mobility as manipulation - design and algorithms of robosimian," *J. Field Robotics*, vol. 32, no. 2, pp. 255–274, 2015.

[3] A. T. Stentz, H. Herman, A. Kelly, E. Meyhofer, G. C. Haynes, D. Stager, B. Zajac, J. A. D. Bagnell, J. Brindza, C. Dellin, M. George, J. Gonzalez-Mora, S. Hyde, M. Jones, M. Laverne, M. Likhachev, L. Lister, M. D. Powers, O. Ramos, J. Ray, D. P. Rice, J. Scheiffflee, R. Sidki, S. Srinivasa, K. Strabala, J. P. Tardif, J.-S. Valois, J. M. Vandeweghe, M. D. Wagner, and C. Wellington, "Chimp, the cmu

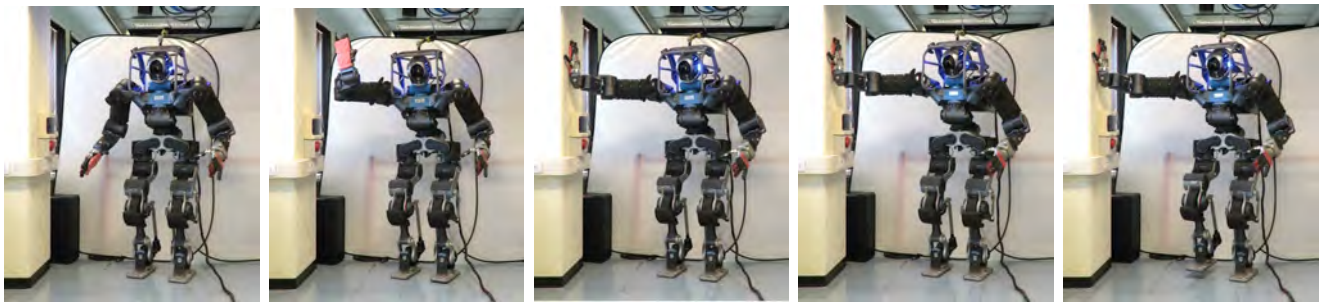

(a) (b) (c) (d) (e)

Fig. 12. Experiment on multi-contact situation, with feet placed on flat terrain. The robot starts in standing configuration (Panels (a)-(b)). After the contact with the wall by the right hand (Panel (c)), the contact force distribution control starts, asking to remove the weight from the right foot. When the task is accomplished (Panel (d)), the operator switch to an inverse kinematic control for lifting up the right foot preserving the CoM (Panel (e)).

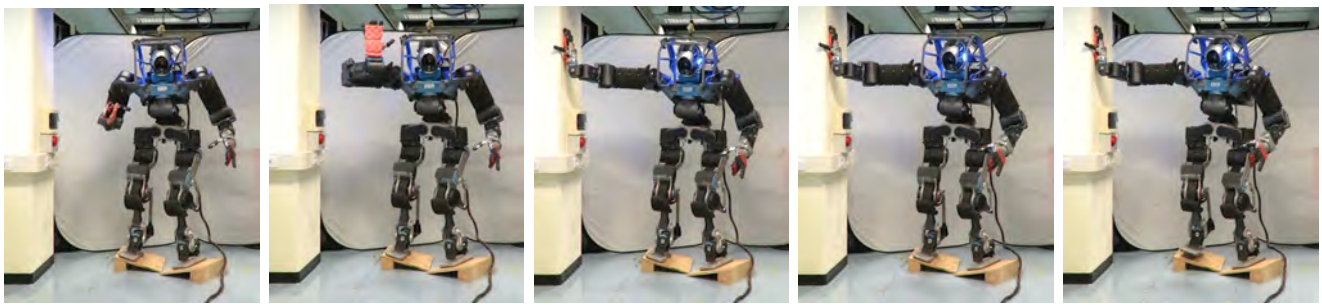

(a) (b) (c) (d) (e)

Fig. 13. Experiment on multi-contact situation, with feet placed on uneven terrain (Fig. 5). The robot starts in standing configuration (Panels (a)-(b)). After the contact with the wall by the right hand (Panel (c)), the contact force distribution control start, asking to remove the weight from the right foot. When the task is accomplished (Panel (d)), the operator switch to an inverse kinematic control for lifting up the right foot preserving the CoM (Panel (e)).

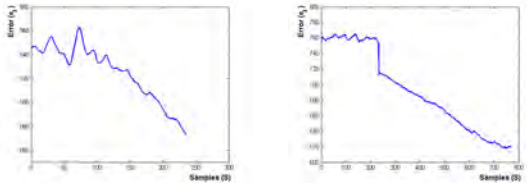

(a) Error evolution relative to the test in Fig. 12, during the transition between three contacts to two contacts condition.

(b) Error evolution relative to the test in Fig. 13, during the transition between three contacts to two contacts condition.

Fig. 14. Error evolutions relative to the tests in Fig.s 12 and 13.

highly intelligent mobile platform," *Journal of Field Robotics (JFR), Special Issue: Special issue on DARPA Robotics Challenge (DRC)*, vol. 32, pp. 209–228, March 2015.

[4] M. Vukobratović and B. Borovac, "Zero-moment point - thirty five years of its life," *International Journal of Humanoid Robotics*, vol. 1, no. 1, pp. 157–173, 2005.

[5] L. Sentis, J. Park, and O. Khatib, "Compliant control of multicontact and center-of-mass behaviors in humanoid robots.," *IEEE Transactions on Robotics*, vol. 26, no. 3, pp. 483–501, 2010.

[6] L. Righetti and S. Schaal, "Quadratic programming for inverse dynamics with optimal distribution of contact forces," in *2012 IEEE-RAS International Conference on Humanoid Robots*, pp. 538–543, 2012.

[7] L. Righetti, J. Buchli, M. Mistry, M. Kalakrishnan, and S. Schaal, "Optimal distribution of contact forces with inverse dynamics control," no. 3, pp. 280–298, 2013.

[8] S.-H. Hyon, J. G. Hale, and G. Cheng, "Full-body compliant human-humanoid interaction: Balancing in the presence of unknown external forces.," *IEEE Transactions on Robotics*, vol. 23, no. 5, pp. 884–898, 2007.

[9] C. Ott, M. Roa, and G. Hirzinger, "Posture and balance control for biped robots based on contact force optimization," in *International Conference on Humanoid Robots*, pp. 26–33, Oct 2011.

[10] B. Henze, C. Ott, and M. A. Roa, "Posture and balance control for humanoid robots in multi-contact scenarios based on model predictive control," in *Intelligent Robots and Systems (IROS 2014), 2014 IEEE/RSJ International Conference on*, pp. 3253–3258, Sept 2014.

[11] A. Bicchi, "On the problem of decomposing grasp and manipulation forces in multiple whole-limb manipulation," *Int. Journal of Robotics and Autonomous Systems*, vol. 13, pp. 127–147, 1994.

[12] A. Bicchi, "On the closure properties of robotic grasping," *The Int. J. of Robotics Research*, vol. 14, no. 4, pp. 319–334, 1995.

[13] M. Gabiccini, E. Farnioli, and A. Bicchi, "Grasp and manipulation analysis for synergistic underactuated hands under general loading conditions," in *International Conference of Robotics and Automation (ICRA)*, pp. 2836 – 2842, 2012.

[14] M. Gabiccini, E. Farnioli, and A. Bicchi, "Grasp analysis tools for synergistic underactuated robotic hands," *International Journal of Robotic Reasearch*, vol. 32, pp. 1553 – 1576, 11/2013 2013.

[15] E. Farnioli, M. Gabiccini, and A. Bicchi, "Optimal contact force distribution for compliant humanoid robots in whole-body loco-manipulation tasks.," in *ICRA*, pp. 5675–5681, IEEE, 2015.

[16] J. B. Sol and T. Asfour, "A whole-body pose taxonomy for loco-manipulation tasks," *CoRR*, 2015.

[17] P. Kaiser, N. Vahrenkamp, F. Schltje, J. Borrs, and T. Asfour, "Extraction of whole-body affordances for loco-manipulation tasks," *International Journal of Humanoid Robotics*, vol. 12, no. 3, pp. 0–0, 2015.

[18] A. A. Shabana, *Computational Dynamics*. New York, NY: Wiley-Interscience Publication, second ed., 2001.

[19] K. Shankar and J. W. Burdick, "Kinematics and methods for combined quasi-static stance/reach planning in multi-limbed robots," in *International Conference on Robotics and Automation, ICRA 2014*.

[20] M. G. Catalano, G. Grioli, E. Farnioli, A. Serio, C. Piazza, and A. Bicchi, "Adaptive synergies for the design and control of the pisa/iit softhand," *International Journal of Robotics Research*, vol. 33, p. 768–782, 2014.

[21] F. Negrello, M. Garabini, M. G. Catalano, J. Malzahn, D. G. Caldwell, A. Bicchi, and N. G. Tsagarakis, "A modular compliant actuator for emerging high performance and fall-resilient humanoids," in *15th IEEE RAS Humanoids Conference (HUMANOIDS2015)*, 2015.